

Identifying relevant positions in proteins by Critical Variable Selection

Silvia Grigolon ^{1,*}, Silvio Franz ^{1,†}, Matteo Marsili ^{2,‡}

¹ *LPTMS - Laboratoire de Physique Théorique et Modèles Statistiques,
Université Paris - Sud, UMR CNRS 8626, 91405 Orsay, France,*

² *Abdus Salam International Center of Theoretical Physics, Strada Costiera 11, 34151 Trieste, Italy**

Evolution, in its course, has found many different solutions to the same problem. Focusing on proteins, the amino acid sequence of protein domains performing the same function in different organisms differs markedly. Since the structure and function of proteins are ultimately encoded in the amino acid sequence, multiple sequence alignments (MSA) of homologous protein domains can be used to provide information about this encoding. Regarding each sequence in an MSA as a solution of an optimisation problem, we exploit the MSA to infer the relevance of different positions, thereby identifying a hierarchy of relevant sites. Our method exploits information on coevolution going beyond pairwise correlations. This method, called Critical Variable Selection (CVS), affords predictions that are significantly different from those of methods based on pairwise correlations, and it recovers biologically relevant sites, including highly conserved ones. As compared to other methods based on pairwise correlations, we find, in the analysed cases, that CVS is more efficient in identifying the core of relevant sites, as well as most of the tightest contacts in the protein tertiary structure.

I. INTRODUCTION

The structure and function that proteins perform inside cells is encoded in their amino acid sequences [1]. Yet sequences are subject to biological evolution, hence the same protein or protein domain may show remarkable differences across organisms that are far apart on the evolutionary tree. What constrains evolution is precisely the requirement that the structure and biological function be conserved [2–4]. This observation lies at the basis of methods for inferring the way in which structure and functions are encoded in the sequence of amino acids by looking at multiple sequence alignments (MSAs) [5]. The problem can be seen as an inverse statistical mechanics problem, where we know that in a sequence of microscopic configurations (the sequences) a certain function is conserved, and we want to infer the “Hamiltonian” specifying how the function is encoded in the sequence. This challenge has attracted a lot of interest [5–7] and, besides its interest for biology, it has become a paradigmatic problem of inference in complex systems.

The frequency of mutations on single sites reveals those positions along the sequence that are “protected” from mutations, either because they are associated to important biological functions or because they are vital for the stability of the tertiary structure. Correlations in the mutation of pairs of sites carry information that can be reverse engineered to reveal contacts in the 3D structure [8–14]. Coevolution on larger subsets of sites can be spotted by an extension of Principal Component Analysis, Statistical Coupling Analysis (SCA) [15], that is able to identify regions that are associated to known functional domains [10, 15].

Yet, in all these examples, inference techniques are limited by and rooted in statistics that do not go beyond pairwise correlations. There are good reasons for that. As higher and higher order correlations are involved, the space of statistical models grows so fast that reliable inference becomes impossible beyond second order statistics, even with very large datasets of sequences. Yet, there is no reason why evolution should use only on pairwise correlations to encode biological function in amino acid sequences. As a matter of fact, selection operates on the whole sequence.

In this paper, we propose a new statistical method going beyond pairwise correlations for the analysis of MSAs of a given protein (domain) family. The method, that we call *Critical Variable Selection* (CVS), is based on the conclusions of Ref. [16] (hereafter MMR) that sampling relevant degrees of freedom of a complex system generates datasets with broad distribution of frequencies, i.e. samples that “look critical”. This conclusion was further refined in Ref. [17] within a Bayesian model selection approach. This paper is the first systematic attempt to exploit these ideas for identifying the subset of relevant positions in a sequence. We introduce the method and its implementation for studying protein sequences and, in order to test its validity, we compare its predictions to those of Statistical Coupling Analysis (SCA) [15] and Direct Coupling Analysis (DCA) [5, 8, 9].

The analysis has been performed on several protein families, but we will focus on two specific families (PF00072 and PF00520), which are of nearly the same length, but differ in the number of available sequences by an order of magnitude. This allows us to probe both methods (SCA and CVS) as the depth of the dataset varies, which is an

* silvia.grigolon@lptms.u-psud.fr; † silvio.franz@lptms.u-psud.fr; ‡ marsili@ictp.it

important dimension. Indeed, despite the recent phenomenal advances in genomic sequencing [18–20], the evolutionary process is necessarily deeply under-sampled. We find that:

1. CVS affords a sharp separation between relevant and irrelevant sites, for a given resolution. This distinction depends in a monotonic manner on resolution[21].
2. Highly conserved sites are typically (but not always) relevant according to CVS.
3. The predictions of CVS are very stable with respect to sample size and can be applied when other methods (e.g. SCA) cannot. CVS predicts meaningful results even for MSA of few hundred of sequences.
4. CVS identifies biologically relevant positions, both functional sites extracted from databases [22, 23] and those identified by DCA.
5. The ranking given by CVS and SCA markedly differs of the top sites. Yet the list of the n most relevant sites predicted by the two methods has a significant overlap when n is large enough, and it contains the biologically relevant sites.
6. When coupled with DCA, CVS is able to identify a core of densely connected residues. All significant contacts predicted by DCA when restricted to the CVS list, turn out to be close on the 3D structure (for PF00072).
7. CVS can be used to improve predictions of contacts by DCA by restricting the analysis only to relevant sites.

In the following we shall first discuss the method and then the results. A final section concludes the paper.

II. RELEVANT POSITIONS IN SEQUENCES AS CRITICAL VARIABLE SELECTION

The idea in MMR is the following: imagine that we can think of each sequence $\vec{s} = (a_1, \dots, a_L)$ of amino acids in the MSA as a realisation of some optimisation problem of a function $U(\vec{s}, \vec{\sigma})$ over an enlarged set of variables that, besides the observed \vec{s} , also includes some unknown variables $\vec{\sigma}$, e.g., reflecting the details of the cellular environment in which that particular sequence has evolved. Under very general conditions, the analysis of [16] shows that a sample of M solutions \vec{s} to this problem with “unknown unknowns”, can be thought of as M independent draws from a probability distribution $p(\vec{s}) \propto \exp[\beta u_{\vec{s}}]$. Then the number of times $k_{\vec{s}}$ that a given sequence \vec{s} occurs in the sample provides a noisy estimate of that part $u(\vec{s}) = E[U(\vec{s}, \vec{\sigma})|\vec{s}]$ of the function that is being optimised which depends on the known variables \vec{s} [24]. In MMR it is argued that the informative content of a given sample is given by the entropy of counts $\hat{H}[K]$, i.e., the entropy of the random variable[25] $K_i = k_{\vec{s}^{(i)}}$ for a randomly chosen sequence $\vec{s}^{(i)}$ in the MSA:

$$\hat{H}[K] = - \sum_k \frac{k m_k}{M} \log \frac{k m_k}{M}, \quad (1)$$

where

$$m_k = \sum_s \delta_{k_s, k}$$

is the number of sequences that occur k times in the MSA. Notice that $\hat{H}[K]$ is different from the entropy of the sequence \vec{s}

$$\hat{H}[\vec{S}] = - \sum_{\vec{s}} \frac{k_{\vec{s}}}{M} \log \frac{k_{\vec{s}}}{M} = - \sum_k \frac{k m_k}{M} \log \frac{k}{M}. \quad (2)$$

Intuitively, $\hat{H}[\vec{S}]$ measures the *resolution* of the description based on \vec{s} whereas $\hat{H}[K]$ measures *relevance*. In the well sampled regime, where each sequence is observed a different number of times ($k_{\vec{s}} \neq k_{\vec{s}'}$ for all $\vec{s} \neq \vec{s}'$, i.e., $m_k = 1 \forall k$), the two measures coincide, i.e. $\hat{H}[\vec{S}] = \hat{H}[K]$. Yet, most of the times one finds itself in the under sampling regime where $\hat{H}[\vec{S}] \geq \hat{H}[K]$.

In practice we would like in this paper to take advantage of these considerations to define sensible positions of MSA data and identify biologically and evolutionarily relevant sites in proteins.

The key observation is that the same construction can be applied to each set of subsequences $\underline{s}_I = (a_i, i \in I)$ specified by some fixed positions ($I \subseteq \{1, 2, \dots, L\}$ is a subset of the positions). This corresponds in dividing the function

$$u(\vec{s}) = u_I(\underline{s}_I) + v_I(\vec{s})$$

in a part u_I that depends only on the subset I of positions and another $v_I(\vec{s})$, depending on the rest. The idea is that relevant variables are indeed those along which the “gradients” $\delta u_I / \delta s_i$ of the function $u(\vec{s})$ are “large”, as s_i varies across the MSA, whereas irrelevant positions are those corresponding to “flat” directions. This is reflected in the statistics and it is quantified by $\hat{H}[K_I]$, where K_I are the random variables associated with the counts of the subsequences \underline{s}_I .

Notice that larger subsets I yield a larger resolution $\hat{H}[\underline{s}_I]$, as the variability of the subsequence can only increase. However, this does not necessarily correspond to an increase in the relevance $\hat{H}[K_I]$ of the subsequence, unless new relevant variables are included. In order to find the most informative positions in a given dataset we propose here to look for the set $I^*(h)$ that maximizes $\hat{H}[K_I]$ for prescribed values h of $H[S]$:

$$I^*(h) = \arg \max_{I: \hat{H}[S]=h} \hat{H}[K_I]. \quad (3)$$

As it was shown in Ref. [16], maximally informative datasets, i.e. that have the largest $\hat{H}[K]$ for a given resolution $\hat{H}[S]$, have critical features (e.g. power law frequency distribution): hence we will call our method *Critical Variable Selection* (CVS).

III. RESULTS

A. The data

In order to test our method, we analyzed two protein families, the response regulator receiver domain (PF00072) and the voltage sensor domain of ion channels (PF00520). The former dataset is made of $N = 62074$ sequences of length $L = 112$ while the latter is made of $N = 6652$ sequences of length $L = 114$, already analyzed respectively in [10] and [26]. For both families the evolutionary spread is quite wide but there is a much better sampling for PF00072 compared to PF00520. For the analysis of tertiary structures, we extracted the .pdb files from the PFAM database [27]: however, the number of available structures is very small and most of them refer to the same sequence [28]. Pdb-accession numbers relative to the structures we analyzed are 1NXW for PF00072 [12] and 3RZV for PF00520.

B. CVS: The algorithm and typical behaviour

To maximize $\hat{H}[K]$, rather than fixing the value of $\hat{H}[S]$, it is more practical to maximize it by fixing the number of positions in the subsequence I , i.e., searching the subsets of n positions

$$I_n^* = \arg \max_{I: |I|=n} \hat{H}[K_I] \quad (4)$$

having maximal relevance. To this aim, we employ a simple gradient ascent algorithm: starting from a random choice of the subset I of n positions, we iterate the following steps:

1. Pick one position $i \in I$ at random and change it to a randomly chosen $i' \notin I$;
2. if $\hat{H}[K_{I'}] \geq \hat{H}[K_I]$, accept the move and $I \rightarrow I' = (I/\{i\}) \cup \{i'\}$ otherwise leave I unchanged.

The algorithm stops after a sufficiently large number of rejections or of moves where $\hat{H}[K_I]$ does not change [29]. Typically, for a given value of n , the algorithm does not produce a single maximum but rather a population of local maxima with similar value of $\hat{H}[K]$, recalling a sort of energy landscape. This protocol thus provides information on the “relevance” landscape of a given sequence. For small n we find that the overlap between different solutions is small and it grows with n . For n sufficiently large we find most of the time the same solution. Fig. 3 illustrates this process as n increases, for the PF00072 family (see caption). This displays the number of times $c_i(n)$ that a particular position i is found in the set I_n^* in 100 repetitions of the algorithm from random initial conditions. An overall measure of the relevance of a site is given by the total count $C_i = \sum_n c_i(n)$. We shall call $c_i(n)$ and C_i counts and total counts, respectively. Fig. 3 shows that there are specific positions which stand out by the plot of counts and

are selected for any value of the subsequence length n . These mostly relevant positions are followed by others arising as the subsequence length increases. However, it must be noticed that there are also some sites that are never selected – the irrelevant ones. The separation between relevant and irrelevant positions is more evident when positions are ranked by decreasing total counts C_i (Fig.1b): after an initial plateau counts quickly approach zero, defining a sharp division between the two sets of positions. The same can be seen in Fig. 3a for PF00520 .

The behaviour of $c_i(n)$ suggests that the set I_n^* grows out of few sites by adding more and more outer layers. This structure is also evident when plotting the “trajectory” of the counts $c_i(n)$ as a function of n for the most relevant positions i (see Fig. 2a). In other words, if a site is selected in the subset of the n most relevant sites by CVS, it will typically be selected also in subsets of $n' > n$ sites. This is a non-trivial fact, which is consistent with the existence of a ranking in terms of relevance, that is independent of n .

Fig. 3b shows that sites selected by CVS include the most conserved sites for PF00520 . This is also true for PF00072 , where however we also find sites that are highly conserved – e.g. 112 which is the 10th most conserved – but which do not rank high in the CVS list of relevant sites. Interestingly, this site (together with 24) has a non-monotonous dependence of $c_i(n)$ on n (not shown in Fig. 2a) and it does not carry relevant biological information, because it is dominated in the MSA by gaps.

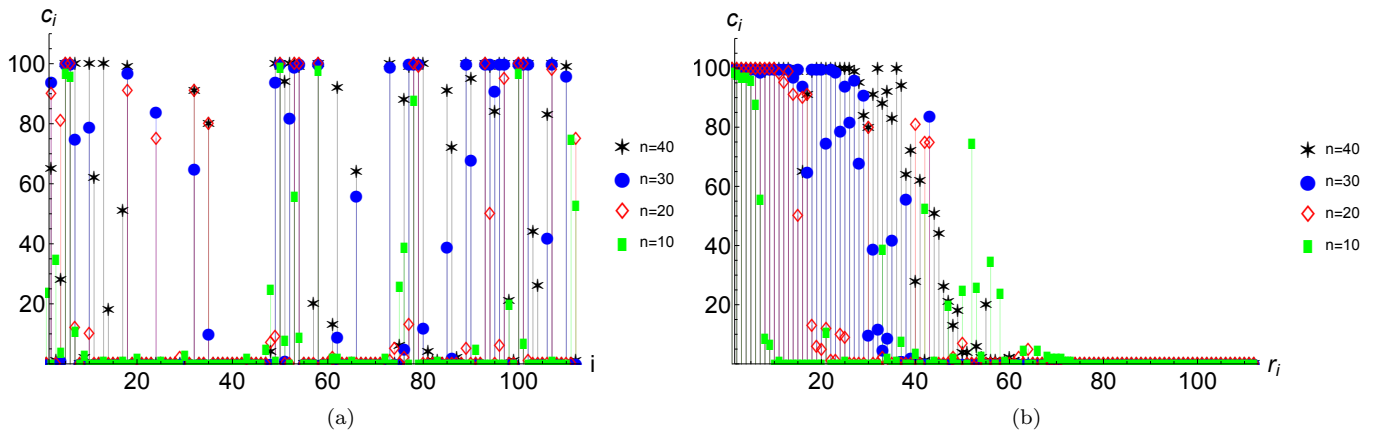


FIG. 1: Relevance count $c_i(n)$ for each position in PF00072 . This is defined as the number of times a particular position i is found in the solution $i \in I_n^*$ for a given n . The algorithm was run for 100 times for $n = 10, 20, 30$ and 40. 1a) $c_i(n)$ versus $i = 1, \dots, L = 112$; 1b) $c_i(n)$ versus the rank r_i defined by ordering the positions i in decreasing total count $\sum_n c_i(n)$ order.

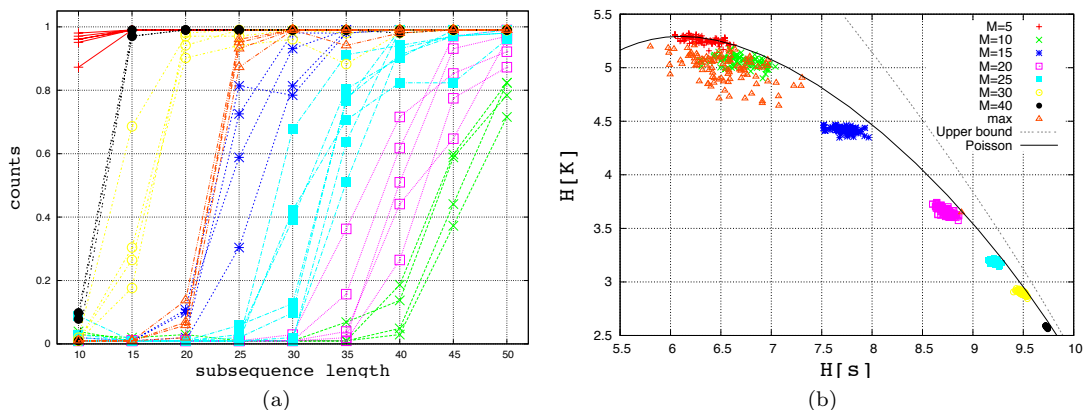


FIG. 2: 2a) Relevance count $c_i(n)$ as a function of n for the most relevant positions in PF00072 . 2b) $H[K]-H[s]$ values relative to the relevance counts $c_i(n)$ in Fig. 2a.

The example of PF00520 shows that even with moderately large MSA, CVS is able to extract stable results that, as we shall see later, have clear biological relevance. In order to further examine the dependence of the prediction of

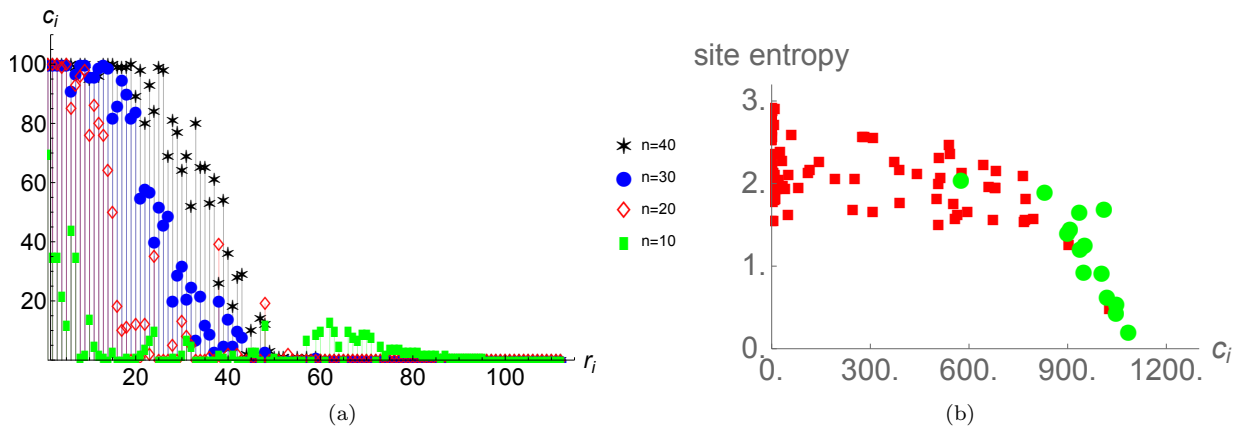


FIG. 3: 3a) Ranked relevance count $c_i(n)$ for positions in PF00520 . The algorithm was run for 100 times for $n = 10, 20, 30$ and 40 . 3b) Site entropy as a function of total count. Circles represent positions identified in the literature (see text).

CVS on the size N of the MSA, we analyzed again the PF00072 cutting the corresponding dataset to about the same number of sequences as in PF00520 . We run CVS for a subset of $N = 6652$ randomly chosen sequences of PF00072 and for an even smaller subset of $N = 666$ sequences. We find that the probability that a position is selected or not both in the full dataset and in the subset is larger than 90% for $N = 6652$ and 76% for $N = 666$ for $n = 40$ and it is even higher for smaller values of n [30]. This suggests that CVS is an adequate inference tool to analyse data in the deep under sampling regime.

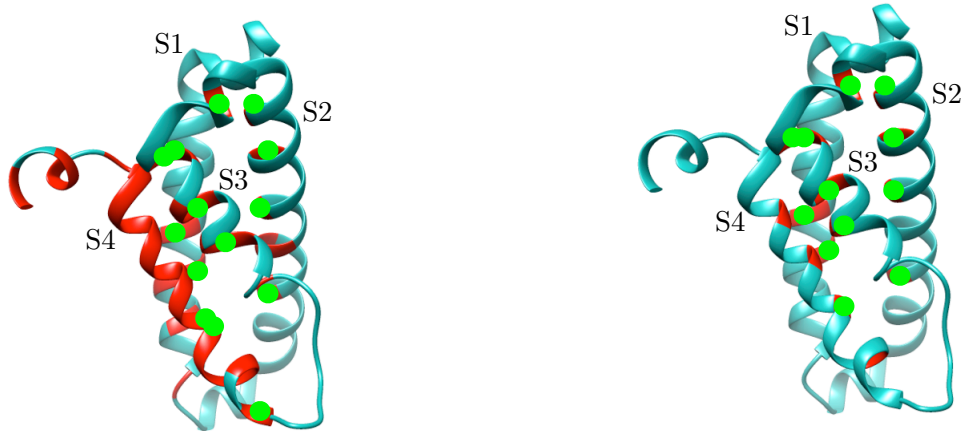
Finally, Fig. 2b) shows that, as anticipated, as n increases, the resolution $\hat{H}[S_{I^*}]$ also increases, but the relevance $\hat{H}[K_{I^*}]$ decreases. As the other plots show, it is necessary to increase the resolution to spot all relevant positions. In practice, we shall rank sites in decreasing order of their counts C_i and to extract a list of n relevant sites, we shall consider the top n sites in this list.

C. Biologically relevant positions

CVS is able to identify biologically relevant sites. The top site identified by CVS for PF00072 coincides with the active phosphorylation site and many of the other relevant sites coincide with biologically relevant ones (see Table I) and are located in the neighbourhood of the active site (see Fig. 6b). We defer a detailed discussion of PF00072 to a later section where we shall compare the prediction of CVS to that of SCA.

Let us now comment on the application of CVS to the Voltage Sensor Domain (VSD) family PF00520 . The VSD is a biological molecular device that transduce electrical signals in cells, e.g. in the control of voltage-gated cation channels. VSD's are composed of four transmembrane segments (S1-S4). We rely on the MSA curated in Palovcak *et al.* [26], whose length $L = 114$ is similar to the one of PF00072 . Since VSD is an highly conserved activation mechanism, protein sequences in the MSA refer to widely different organisms, the evolutionary spread in the PF00520 dataset is as wide as that characterizing PF00072 . Yet the number of available sequences for PF00520 ($N = 6652$) is much smaller compared to the case of PF00072 .

As shown in Fig. 3a, CVS also in this case clearly distinguishes relevant from irrelevant sites as in the case of PF00072 . Fig. 3b shows that, besides highly conserved sites having a clear biological relevance, CVS distinguishes between sites whose variability is evolutionarily related from those that can be regarded as noise. A first group of 13 sites with high counts C_i can be identified. This contains 9 sites identified in Refs. [26, 31]. Three more functionally relevant sites have counts larger than 500 belong to a larger group of the 38 most relevant sites. These sites are represented on the 3D structure in Fig.4. These include N-62, N-72, R-76 and E-93 of the voltage-dependent K^+ channel KvAP which are important for channel function [23, 31]. The same sites have also been identified in Ref. [26], that refer to the NavAb sequence (E-49, E-59, R-63, D-80 respectively). Ref. [26] also highlights the role of I-22, F-56 and F-71 in NavAb and it discusses the application of Direct Coupling Analysis (see later) on the VSD MSA, identifying several evolutionary conserved contacts along the chain. In particular, E-49 is found to be in contact both with N-25 and with E-96, which are far apart in the NavAb structure. Ref. [26] argues that these two contacts are important to confer stability both to the activated and to the resting state of the protein domain. All these sites are found to be relevant in the CVS analysis, as well as R-63 and S-77, which are also found to be in contact on the



(a) Top 40 CVS sites for the PF00520 .

(b) Top 15 CVS sites for the PF00520 .

FIG. 4: Top CVS sites got for the PF00520 . Green circles spot the functional sites already identified in Refs. [23, 31] as discussed in the Main Text.

Uniprot sites	Our sites	Function	SCA	CVS
10	5	active	✓	✓
11	6	active	✓	✓
56	52	active, phosphorylation	✓	✓
64	60	active	X	X
84	80	active	✓	✓
101	99	active	✓	(100)
104	102	active and dimerization interface	✓	✓
105	103	active and dimerization interface	(102)	✓
106	104	active and dimerization interface	(105)	(103)
60	56	intermolecular recognition site	✓	X
59	55	intermolecular recognition site	(56)	(54)
62	58	intermolecular recognition site	(57)	✓
63	59	intermolecular recognition site	X	(58)
64	60	intermolecular recognition site	X	X

TABLE I: Functional sites extracted from [22, 23] for the B4DA37.9BACT sequence. In order to make a consistent comparison sequences have been matched with particular attention to the gaps.

NavAb structure. Ref. [26] also reports a false positive contact (between W-76 and T-15). We find that while W-76 is relevant, T-15 is not ($C_{T-15} = 145$). Finally, we find an enrichment in relevant sites in the region corresponding to S4, which is a highly dynamical region of the VSD, and in the S2-S3 turn (Tyr-63 to Pro-95 in KvAP) that has been suggested to be structurally important [31].

D. Comparison with SCA

In order to gauge the relevance of the list of sites extracted by the CVS algorithm, we compare them with those obtained by the so-called Statistical Coupling Analysis (SCA) [15].

Statistical Coupling Analysis (SCA) is a well-known technique aimed at undressing datasets from sampling noise, in order to extract relevant information in protein sequences. A detailed description of the method is given in the Appendix. In brief, SCA merges Principal Component Analysis with a noise cleaning procedure. It is based on the correlation matrix built using single and double amino acid frequencies at each position, enhanced as in Ref. [15] to highlight positional conservation and restricted to the set of positions by taking the Frobenius norm (see Appendix). In order to undress the matrix from the noise arising from the finiteness of the sample, a random correlation matrix is built from a reshuffled MSA with the same single amino acid frequencies at each position. If some kind of information

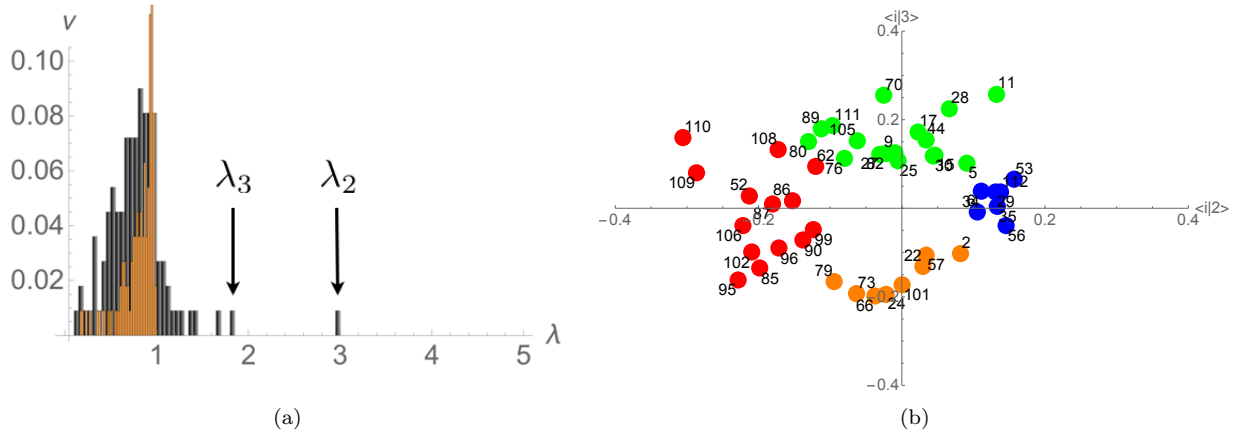


FIG. 5: 5a) Histogram of the eigenvalues distribution relatively to the random matrix \mathcal{M}_{ij} (orange blocks) and to the actual correlation matrix \hat{C}_{ij} (black blocks). The highest one, $\lambda_1 \simeq 24.5$ is neglected [15]. In the analysis, we focused on the other two highest ones, i.e., $\lambda_2 \simeq 3$ and $\lambda_3 \simeq 1.8$, since the corresponding eigenvectors components turn out to be noisier as the eigenvalues approach the random bulk. 5b) The four sectors identified in the PF00072 represented in the plane spanned by the eigenvectors $|2\rangle$ and $|3\rangle$. Each site is labeled according to its position along our MSA.

is enclosed in the protein sequence, one expects to find remarkable differences between the randomized and the actual matrix. Comparing the eigenvalue distribution of the actual and the random matrix, it is possible to identify the *principal components* as the eigenvalues corresponding to those of the actual correlation matrix clearly standing out of the distribution of the eigenvalues of the randomised matrix. This is illustrated in Fig. 5a) for PF00072. Each position along the sequence can then be represented as a point in the space spanned by the principal components, whose coordinates are the components of the eigenvectors corresponding to that position. The distance of each point from the origin can be taken as a measure of relevance of the corresponding site, according to SCA.

Fig. 5b plots the first 46 points in this list for PF00072 in the space spanned by the 2nd and 3rd principal components (as discussed in [15], the largest eigenvalues should not be considered since it is purely a signature of the phylogenetic history of the dataset). Performing a clustering procedure onto this set, one finally gets groups of mostly correlated sites, usually called *sectors* in the literature [10, 15] (see Appendix I for details).

For PF00072 four sectors can be identified, that correspond to functional domains on the tertiary structure (Fig. 6a) (pdb-file 1NXW, [27]). They have also been compared with functional sites extracted from databases: this point will be further discussed in the next section.

For PF00072, when the list of the n most relevant sites according to SCA is compared to that generated by CVS we find zero overlap as long as $n \leq 18$. This is not surprising: principal component analysis is tailored to identify the most relevant drivers of variation in a data-set, which is why highly conserved sites do not appear on top of the list of relevant sites, according to SCA. This implies that SCA and CVS are qualitatively very different methods. Yet, when one compares the lists for larger number n of top sites, the overlap sharply increases. We shall concentrate below on the comparison between the top $n = 41$ sites in the two lists[32], which is approximately where the overlap between the two lists is largest ($\sim 54\%$) as compared to what one would obtain if sites were chosen randomly ($\sim 37\%$).

We found that SCA is much more difficult to implement for PF00520: because of the high diversity of the sample and the few sequences ($N = 6652$), the tails of the distribution of the random matrix eigenvectors' components are very broad, and the eigenvector components very noisy. This prevents a reliable application of the method. Barring all this and imposing a conservative threshold, one can select 5 top sites, four of which highly conserved (F-56, D-80, R-99 and R-102 on NavAb) with a large relevance count and one (A-112) highly variable, with a moderately large CVS count. In what follows, we shall confine our discussion of the comparison between CVS and SCA to the case of PF00072, where statistics is definitely enough for the latter method to produce stable results.

Let us now compare the lists of the 41 top sites identified by SCA and CVS for PF00072. It is instructive to analyze the positions of the selected sites on the tertiary structure. We analyzed one structure (1NXW) whose results are shown in Fig. 6. Many common domains on the α -helices and β -sheets are clearly identified by both methods (red bands) with few differences, e.g. the central β -sheet identified by CVS but not by SCA.

In order to understand if CVS is able as well as SCA to detect functional domains, we extracted functional sites from the UniProtKB and NCBI-RefSeq databases [22, 23]. The results are shown in Tab. I where one can see that

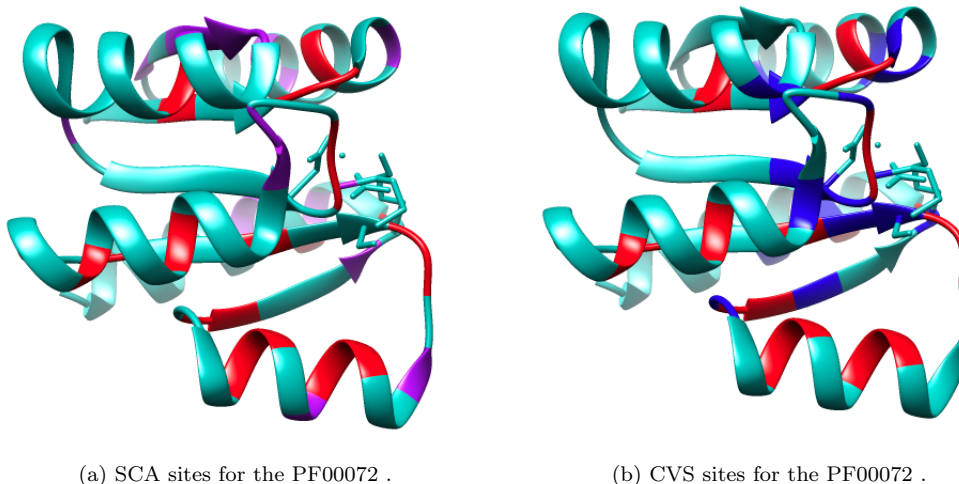


FIG. 6: Sites obtained by SCA (Fig. 6a) and CVS (Fig. 6b) represented on the tertiary structure with the overlap in red.

most of the sites are detected by both methods. In 4 cases each method selects nearest neighbors instead of the site itself and failed to identify two sites (63,64 for SCA and 60,64 for CVS) as relevant.

In summary, both CVS and SCA are able to detect functionally relevant sites and the same domains with slight differences. In order to investigate the nature of these differences we shall resort to Direct Coupling Analysis in the next subsection.

E. Direct Coupling Analysis: interaction networks and hidden variables

Direct Coupling Analysis (DCA) is a method aimed at identifying a network of interactions between positions along a protein domain, that are inferred from the traces left by the evolutionary process on the pair correlation matrix. In recent years many efforts have been spent in refining this observation into a quantitative bio-informatic tool [8–14]. Given the MSA of a certain protein family, DCA produces an F-score $F_{i,j}$ for each pair of positions $i, j = 1, \dots, L$ with $F_{i,i} = 0$. In particular, if two positions are relevant for preserving the tertiary structure, by establishing a physical contact, one expects residues on these sites to co-evolve, that results in a large value of $F_{i,j}$. DCA is indeed a powerful tool for predicting contacts in protein domains.

Here we use DCA to generate a network of interactions between positions, with the goal of deriving an independent assessment of the relevance of the sites selected by CVS and SCA, respectively. Therefore, we stick with a standard implementation of DCA – the so called *naïve Mean Field Direct Coupling Analysis* (DCA) based on the *Plefka expansion* [33] – that has been shown to capture most of the direct contacts in 3D protein structures [9]. We refer to the appendix for a concise discussion of the steps leading to the calculation of $F_{i,j}$ as applied to our dataset. We confine our analysis to PF00072 for which both CVS and SCA yield stable predictions.

We performed DCA on the whole protein and then on the CVS and the SCA lists of sites to infer the $F_{i,j}$ scores between the amino acids. We shall call them respectively $F_{i,j}^{all}$, $F_{i,j}^{CVS}$ and $F_{i,j}^{SCA}$.

A first comparison between the two lists can be made by selecting the n most relevant sites on each list and the network defined by the m top interactions from the list of $F_{i,j}^{all}$. Figs. 7a, 7b shows the resulting network for $n = 41$ and $m = 200$ for the CVS and SCA lists, respectively. Only a fraction of the m selected links will connect two of the n top sites of a given list, so the density of links and the fragmentation of the resulting networks provide a measure of “positional” relevance of the selected sites. Visual inspection reveals that CVS sites are more densely connected both in terms of number of links and of size of the largest connected component, and less fragmented, meaning that CVS sites are more interacting than those selected by SCA. This conclusion holds true for all relevant values of n and m . Furthermore, the number of links between the n selected sites and the $L - n$ remaining ones is smaller for the CVS than for SCA list, for most values of m . We also notice that, for SCA, sectors do not seem to be related to a motif pattern in the network (Fig. 7b).

Secondly, Fig. 8 shows that, when restricted to the CVS list, pairs of sites with a large $F_{i,j}$ correspond to close

sites, whereas the same is not true always for the SCA list. For example, Asp 96-Thr 100 and Lys 81-Pro 74, whose distances are respectively about 11.4 Å and 17.3 Å, turn out to have values of $F_{i,j}^{SCA} \approx 4$. In general, Fig. 8 shows that, when DCA is run on the reduced list, the same value of $F_{i,j}$ correspond to pairs of sites which are in a narrower range of distances in the case of CVS than in the case of SCA.

Indeed, when run on a subset \mathcal{L} of sites, DCA predicts higher values of $F_{i,j}^{\mathcal{L}}$ as compared to the unrestricted case $F_{i,j}^{all}$. We observe this effect both for CVS and for SCA, where $F_{i,j}^{\mathcal{L}} \approx 1.2F_{i,j}^{all}$. (Fig. 9). The amplification in the couplings $\delta F_{i,j}^{\mathcal{L}} = F_{i,j}^{\mathcal{L}} - F_{i,j}^{all}$ can be due to two reasons: on one side, we expect that if irrelevant nodes are eliminated, the estimate of the interaction between nodes in \mathcal{L} improves. On the other, as shown schematically in Fig. 10, if nodes $k \notin \mathcal{L}$ that interact strongly with both i and j are eliminated, the estimate of $F_{i,j}$ will increase to account for the missing interactions of i and j with the “hidden node” k . In order to distinguish between amplification of interactions due to genuine noise reduction and the effect of hidden nodes, we compare the increase $\delta F_{i,j}^{\mathcal{L}}$ in the interaction with the quantity

$$\Delta F_{i,j} = F_{ij}^{all} - \max_{k \notin \mathcal{L}} \min(F_{ik}^{all}, F_{jk}^{all}) \quad (5)$$

for all $i, j \in \mathcal{L}$. In words, a negative value of $\Delta F_{i,j}$ implies that the enhancement $\delta F_{i,j}^{\mathcal{L}}$ in the coupling is due to the neglect of hidden variables rather than to noise reduction (see Fig. 10).

Fig. 11 plots $\delta F_{i,j}^{\mathcal{L}}$ versus $\Delta F_{i,j}$ for contacts among sites in the CVS list and in the SCA list. The histograms along the axis in Fig. 11 also shows the distribution of $\Delta F_{i,j}$ and $\delta F_{i,j}^{\mathcal{L}}$ for lists of 41 randomly chosen sites. With respect to this, the distribution of $\Delta F_{i,j} > 0$ for contacts between CVS sites is significantly shifted towards positive values, much more than for the SCA case. The presence of many contacts with $\Delta F_{i,j} > 0$ in the CVS list suggests that DCA is not severely affected by hidden variables, when restricted to the CVS list. CVS may be then used as a pre-processing noise-undressing step in DCA.

This conclusion is further corroborated by the analysis of the network of contacts between hidden variables. Given a list \mathcal{L} of putatively relevant sites, we define a site $k \notin \mathcal{L}$ a hidden variable if *i)* $k \notin \mathcal{L}$ and *ii)* there exist at least a pair of sites $i, j \in \mathcal{L}$ with $F_{i,j}^{\mathcal{L}} > 2$ and $|i - j| > 2$ for which $\Delta F_{i,j} < 0$, with the maximum in Eq. (5) being attained at site k . As illustrated in Fig. 10, hidden variables are those sites that “explain” spurious contacts[34]. The network of hidden variables for the CVS list is smaller, more fragmented and less densely connected than that of the SCA list (figure not shown). The latter in turn, can hardly be distinguished from the network of hidden variables obtained for random lists of the same number of nodes[35].

IV. DISCUSSION

In summary, we have proposed a new method for the identification of relevant sites in protein domains. Given a multiple sequence alignment (MSA) for a given protein family, the method is based on finding those subsets of n positions for which the entropy $H[K]$ of the frequency with which different subsequences occur is maximal. Its implementation is straightforward and does not require any further data-processing step.

We have discussed the application of the method to two protein domain families, the response regulator receivers (PF00072) and the ion channels (PF00520), being this latter a smaller dataset than the former. By starting with different subsequences length, the method assigns to each position a *count* that can be used to assess the relevance (respectively irrelevance) of a certain site. As the subset length includes enough positions, CVS affords a sharp separation between relevant and irrelevant sites for all the datasets we analysed, being them often, i.e. not always, highly conserved positions. Besides, site relevance turns out to be monotonic with the subset length and typically if a site i is selected as relevant in the subset of the n most relevant positions, it will be very likely selected in the subset of $n' > n$ sites as well.

CVS is furthermore able to identify biologically relevant positions: the sites extracted from [22, 23] or identified by inference methods as Direct Coupling Analysis turn out to be tagged as relevant by our method for both PF00072 and PF00520. The latter dataset, as previously discussed, has allowed us to assess the stability of the method with respect to the sample size: the ion channel dataset lies indeed in the deep under sampling regime (few number of sequences characterized by high diversity) and methods as SCA are not able to give enough predictions about it. Nonetheless, we have shown that CVS can still give meaningful results in agreement with biological predictions [23, 31].

We have as well compared CVS results with those one gets by applying Statistical Coupling Analysis (SCA), showing the two methods give deeply different results. The comparison has been performed on the PF00072 dataset as on the other one we have discussed the difficulties one encounters while applying SCA. Although the two methods show remarkably different results, in order to give consistently comparisons, the subsets of lists that maximally overlap have been taken into account: we have shown that in both cases one is able to recover biologically relevant information. Yet, differences between CVS and SCA results can be furthermore highlighted by using Direct Coupling Analysis

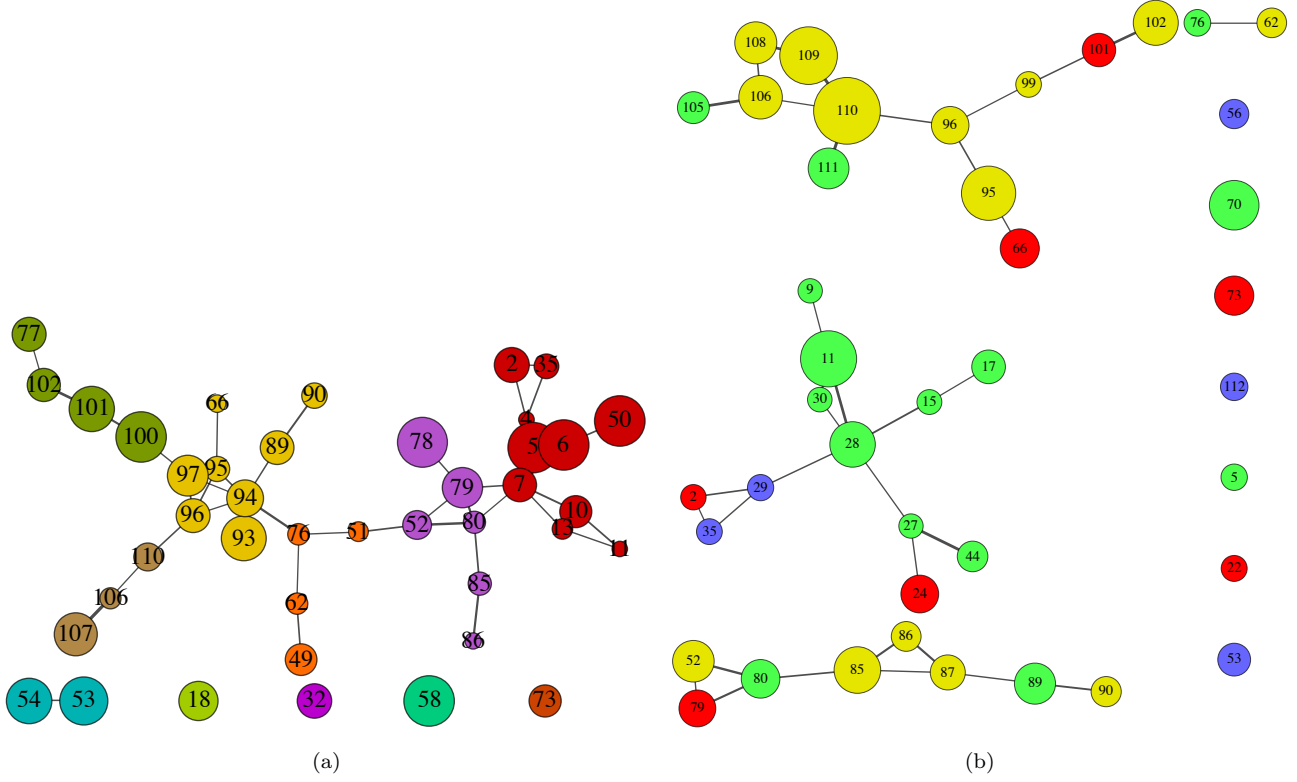


FIG. 7: 7a) Network representation of the CVS sites with communities highlighted by the Mathematica Network Analysis package. The size of the nodes is rescaled with their CVS counts, C_i , and their links are those obtained with the nMFDCA, rescaled as well according to their own intensity. Just the top 200 couplings have been taken into account. 7b) Same representation as in 7a) but for the SCA sites. Colours are now defined according to the sectors (first one in blue, second red, third green and fourth yellow).

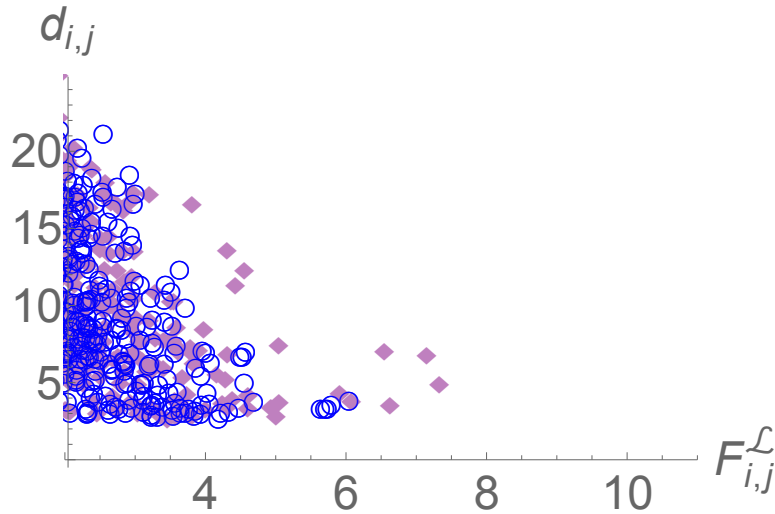


FIG. 8: Distance on the tertiary structure $d_{i,j}$ as a function of $F_{i,j}^{\mathcal{L}}$ for all the couples in the $\mathcal{L} = \text{CVS}$ and $\mathcal{L} = \text{SCA}$ (respectively blue empty circles and purple diamonds) lists. Distance on the tertiary structure $d_{i,j}$ as a function of $F_{i,j}^{\text{CVS}}$ for all the couples in the CVS list (blue empty circles). Only pairs of sites with $F_{i,j}^{\text{CVS}} > 2$ and at a distance $|i - j| > 2$ along the primary structure are shown. In the same plot, purple diamonds refer to $d_{i,j}$ vs $F_{i,j}^{\text{SCA}}$, again for $F_{i,j}^{\text{SCA}} > 2$ and $|i - j| > 2$.

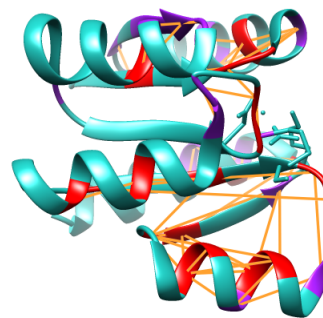
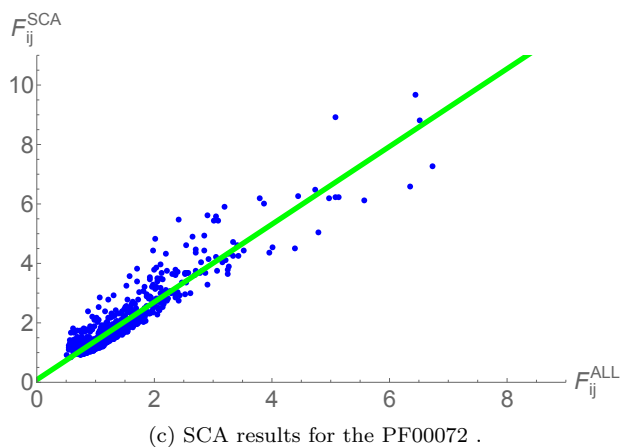
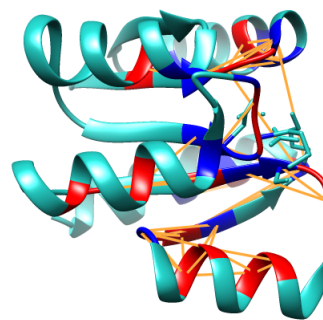
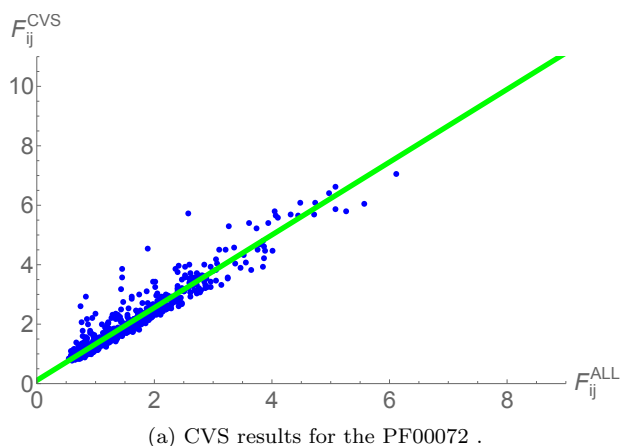


FIG. 9: Couplings got through nMFDCA on the sublists of CVS sites (Fig. 9a) and of SCA sites (Fig. 9c) versus the corresponding couplings obtained through the nMFDCA over the whole protein, F_{ij}^{all} , together with a fit line. Besides the amplification of the couplings, the top 30 contacts above the green line are represented on the tertiary structure of the PF00072, respectively for the CVS results (Fig. 9b) and for the SCA ones (Fig. 9d). However SCA results stay still noisy and between the top contacts amplifies at least two false positives, i.e., is respectively about 11.4 Å (Asp 96-Thr 100) and 17.3 Å (Lys 81-Pro 74).

(DCA). CVS identifies a core of densely connected residues and all significant contacts predicted by DCA on the restricted lists turn out to be close on the 3D structure for the PF00072 .

By finally analysing how the output of DCA inferred on the lists of selected residues correlates with their distance on the tertiary structure, we have been allowed to build up a network framework of relevant sites showing that CVS identifies a core of densely connected residues. At the same time, the effect of hidden variables, which is unavoidable when DCA inference is limited to a subset of contacts, is greatly reduced among variables identified by CVS both with respect to those identified by SCA and with respect to randomly chosen sites. This further corroborates the conclusion that CVS indeed singles out subsets of relevant sites in protein domains.

We stress, in particular, the fact that CVS is able to recover insights from methods based on single site conservation and pairwise correlation. Yet, the most exciting aspect of CVS lies precisely in its ability to probe the co-evolutionary process beyond single site conservation and pairwise correlation. This calls, on one hand, for the development of inference methods going beyond pairwise interactions, and on the other hand to applications of CVS to instances that may lead to a more critical assessment of its potential for reverse engineering evolutionary processes.

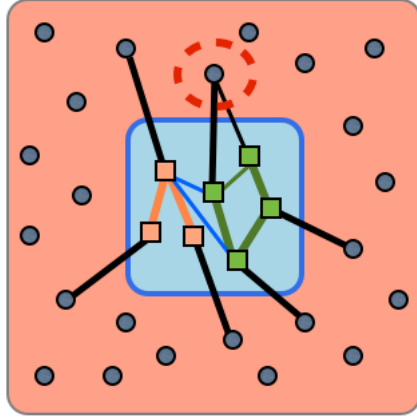


FIG. 10: Pictorial representation of the network between sites in a protein domain. The subset of sites in the light blue subset square correspond to those on a list \mathcal{L} of “putatively” relevant sites, whereas those in the outer orange shaded area correspond to neglected sites $k \notin \mathcal{L}$. The thickness of links represents the strength $F_{i,j}$ of interaction. An example of an hidden variable is highlighted by the red dashed circle.

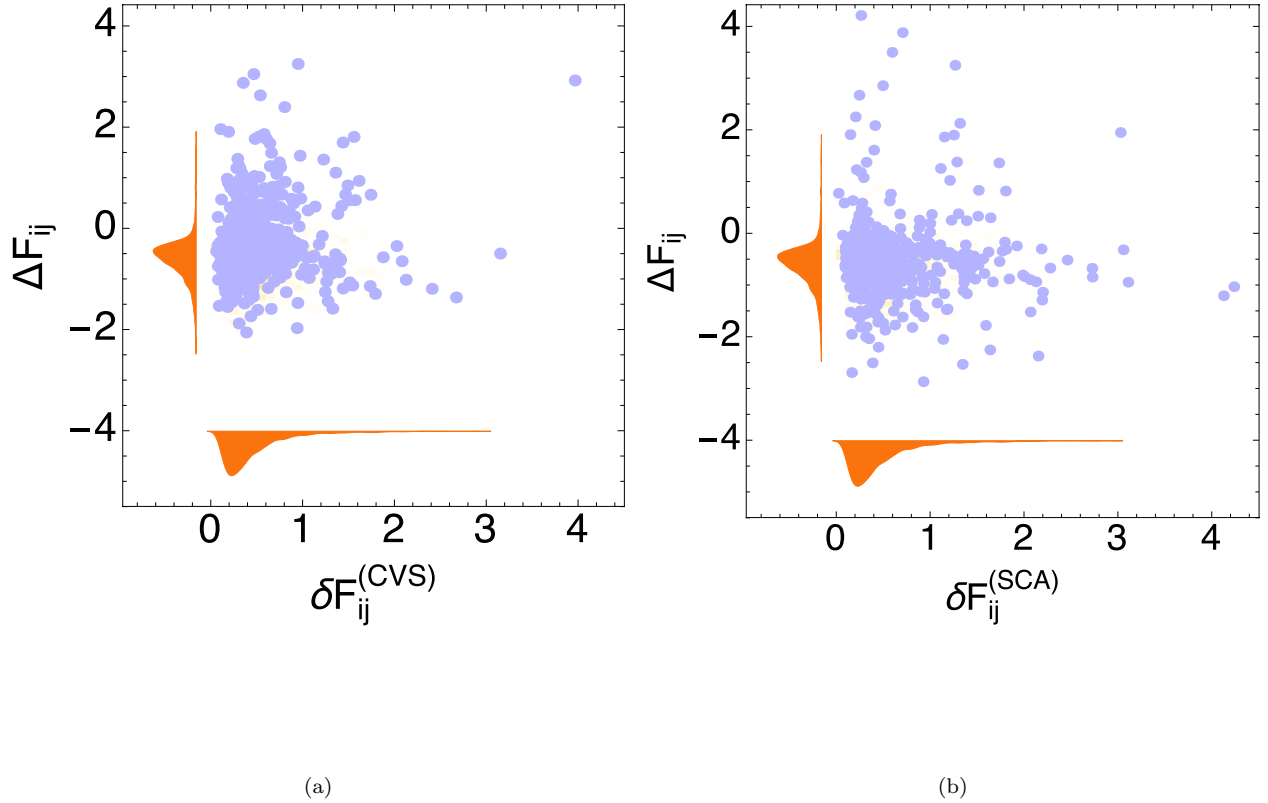


FIG. 11: ΔF_{ij} plotted as a function of $\delta F_{ij}^{\mathcal{L}}$ for both the CVS (Fig. 11a) and the SCA (Fig. 11b) results. The difference between the two scenarios is pretty evident, being the latter more biased towards negative values of ΔF_{ij} , meaning that there are tight contacts with sites not selected by SCA. The histograms on the axis in both figures represent the distributions of the two quantities obtained by using 5 random lists.

ACKNOWLEDGMENTS

We thank Sébastien Boyer, Alice Coucke and Eleonora De Leonardis for helpful suggestions, Vincenzo Carnevale and Daniele Granata for interesting discussions and for providing the data on PF00520, Matteo Figliuzzi, Yasser Roudi, Pierpaolo Vivo and Martin Weigt for insightful discussions. This work was supported by the Marie Curie Training Network NETADIS (FP7, 290038).

-
- [1] L. Stryer J. M. Berg, J. L. Tymoczko. *Biochemistry*. W. H. Freeman, 5th edition, 2002.
- [2] J. Overington M. S. Johnson A. Sali T. L. Blundell. Tertiary structural constraints on protein evolutionary diversity: templates, key residues and structure prediction. *Proc. R. Soc. B*, 241(132-145), 1990.
- [3] A. A. Fodor R. W. Aldrich. On evolutionary conservation of thermodynamic coupling in proteins. *J. Biol. Chem.*, 279(18):19046–19050, 2004.
- [4] M. Socolich S. W. Lockless W. P. Russ H. Lee K. H. Gardner R. Ranganathan. Evolutionary information for specifying a protein fold. *Nature*, 437:512-518, 2005.
- [5] B. Lunt H. Szurmant A. Procaccini J. A. Hoch T. Hwa M. Weigt. Inference of direct residue contacts in two-component signaling. *Methods in Enzymology*, 471:17, 2010.
- [6] J. D. Bryngelson P. G. Wolynes. Spin glasses and the statistical mechanics of protein folding. *PNAS*, 84:7524–7528, 1987.
- [7] R. A. Goldstein Z. A. Luthey-Schulten P. G. Wolynes. Optimal protein-folding codes from spin-glass theory. *PNAS*, 89:4918–4922, 1992.
- [8] M. Weigt R. A. White H. Szurmant J. A. Hoch T. Hwa. Identification of direct residue contacts in protein-protein interaction by message passing. *PNAS*, 106(67):72, 2009.
- [9] F. Morcos A. Pagnani B. Lunt A. Bertolino D. S. Marks C. Sander R. Zecchina J. N. Onuchic T. Hwa M. Weigt. Direct-coupling analysis of residue coevolution captures native contacts across many protein families. *PNAS*, 108(49):E1293–1301, 2011.
- [10] S. Cocco R. Monasson M. Weigt. From principal component to direct coupling analysis of coevolution in proteins: Low-eigenvalue modes are needed for structure prediction. *PLoS Computational Biology*, 9(8):e1003176, 2013.
- [11] M. Ekeberg C. Lövkvist Y. Lan M. Weigt E. Aurell. Improved contact prediction in proteins: Using pseudolikelihoods to infer potts models. *Phys. Rev. E*, 87:012707, 2013.
- [12] C. Baldassi M. Zamparo C. Feinauer A. Procaccini R. Zecchina M. Weigt A. Pagnani. Fast and accurate multivariate gaussian modeling of protein families: predicting residue contacts and protein - interaction partners. *PLoS One*, 9(3):e92721–33, 2014.
- [13] C. Feinauer M. J. Skwark A. Pagnani E. Aurell. Improving contact prediction along three dimensions. *PLoS Computational Biology*, 10(10):e1003847, 2014.
- [14] M. Ekeberg T. Hartonen E. Aurell. Fast pseudolikelihood maximization for direct-coupling analysis of protein structure from many homologous amino-acid sequences. *J. Comput. Phys.*, 276(341-356), 2014.
- [15] N. Halabi O. Rivoire S. Leibler R. Ranganathan. Protein sectors: Evolutionary units of three-dimensional structure. *Cell*, 138:774–786, 2009.
- [16] M. Marsili I. Mastromatteo Y. Roudi. On sampling and modeling of complex systems. *J. Stat. Mech.*, P09003, 2013.
- [17] Ariel Haimovici and Matteo Marsili. Criticality of relevant descriptions in the under-sampling domain. arXiv:1502.00356 [physics.data-an], Jan 2015.
- [18] F. Ozsolak P. M. Milos. Rna sequencing: advances, challenges and opportunities. *Nature Reviews Genetics*, 12:87–98, 2011.
- [19] E. R. Mardis. A decade’s perspective on dna sequencing technology. *Nature*, 470:198–203, 2011.
- [20] I. Pagani K. Liolios J. Jansson I. Chen T. Smirnova et al. The genomes online database (gold) v.4: status of genomic and metagenomic projects and their associated metadata. *Nucleic Acids Res*, 40:D571, 2012.
- [21] This is consistent with the existence of an underlying ranking in relevance that CVS is probing.
- [22] The UniProt Consortium. Activities at the universal protein resource (uniprot). *Nucleic Acids Res.*, 42:D191–D198, 2014.
- [23] Bethesda (MD). *The Reference Sequence (RefSeq) Project Chapt. 18*. The NCBI handbook. National Library of Medicine (US), National Center for Biotechnology Information, 2002.
- [24] Here $E[\dots|\vec{s}]$ is meant to be an expectation on all the unknown unknowns, keeping \vec{s} fixed.
- [25] We use uppercase for random variables defined on the space of sequences of the MSA, where each sequence has the same probability. Also we assume maximum likelihood estimates of the probability, so $P\{\vec{S} = \vec{s}\} = k_{\vec{s}}/M$ and $P\{K = k\} = km_k/M$.
- [26] E. Palovcak L. Delemotte M. L. Klein V. Carnevale. Evolutionary imprint of activation: the design principles of vsds. *J. Gen. Physiol.*, 143(2):145–156, 2014.
- [27] R. D. Finn A. Bateman J. Clements P. Coggill R. Y. Eberhardt S. R. Eddy A. Heger K. Hetherington L. Holm J. Mistry E. L. L. Sonnhammer J. Tate M. Punta. The pfam protein families database. *Nucleic Acids Research*, (Database Issue 42):D222–D230, 2014.

- [28] H. M. Berman G. J. Kleywegt H. Nakamura J. L. Markley. The protein data bank at 40: Reflecting on the past to prepare for the future. *Structure*, 20:391–396, 2012.
- [29] The logic behind the procedure is the same as that of the Kawasaki algorithm at $T = 0$ for a spin system [?].
- [30] Let p_i and q_i be the estimated probabilities that position i is selected in the full dataset and in the subset of sequences, respectively. Then the probability that position i is either present or not in both datasets is $p_i q_i + (1 - p_i)(1 - q_i)$. The estimate in the text refers to the average over i of this probability, i.e. to a randomly chosen position i .
- [31] S.Y. Lee A. Lee J. Chen R. MacKinnon. Structure of the kvap voltage-dependent k^+ channel and its dependence on the lipid membrane. *PNAS*, 102(43):15441, 2005.
- [32] Since, sequence alignment procedures introduce gaps, we remove those sites that result in gaps in the consensus sequence. The number of selected gaps was very low, less than the 8% in both cases.
- [33] T. Plefka. Convergence condition of the tap equation for the infinite-ranged ising glass model. *J. Phys. A.: Math. Gen.*, 15:1971, 1982.
- [34] Here contacts are defined as pairs of sites with $F_{i,j}^{\mathcal{L}} > 2$ between sites that are at a distance $|i - j| > 2$ of more than two residues on the primary structure. The latter excludes sites that have large F -score because they are close along the amino acid sequence. We say that the contact is spurious if $\Delta_{i,j} < 0$) when DCA is restricted to the list \mathcal{L} . The threshold on $F_{i,j}$ or on the distance along the primary sequence are clearly arbitrary, but they serve to prune the set of hidden variables from idiosyncratic effects.
- [35] For CVS we find 31 hidden variables. Taking the top 200 DCA contacts, we find that these 31 nodes form a network that has 4 disconnected components, the largest of 23 nodes, with an average degree of 2.84. For the SCA list, we find 43 hidden variables, and the top 200 DCA contacts connect these in a single connected component of average degree 3.95. For random lists of $n = 41$ sites, we found 40 ± 5 hidden variables, all in a single connected component, with average degree ≈ 4.4 .
- [36] V. A. Marchenko L. A. Pastur. Distribution of eigenvalues for some sets of random matrices. *Mat. Sb.*, 1(4):457–483, 1967.
- [37] O. Rivoire. Elements of coevolution in biological sequences. *Phys. Rev. Lett.*, 110:178102, 2013.

Appendix A: Statistical Coupling Analysis in a nutshell

In this section we are going to give an overview of Statistical Coupling Analysis as applied onto our datasets.

Let us consider a MSA as an ensemble of N sequences $\vec{s}^\alpha = \{s_1^\alpha, \dots, s_L^\alpha\}$ of length L where each s_i^α ($\alpha = 1, \dots, N$ and $i = 1, \dots, L$) represents either an amino acid or a gap (or an uncertain letter as well) and can then take $q = 21$ values. A first measure of conservation throughout the dataset is given by the frequency of the amino acid a at position i , i.e.:

$$f_i^a \equiv \frac{1}{N} \sum_{\alpha=1}^N \delta_{a,s_i^\alpha}.$$

Pair - frequencies can then be defined in a straightforward manner, as:

$$f_{ij}^{ab} \equiv \frac{1}{N} \sum_{\alpha=1}^N \delta_{a,s_i^\alpha} \delta_{b,s_j^\alpha},$$

that gives a measure of the simultaneous appearance of the amino acids a and b respectively at positions i and j . The *correlation matrix* C_{ij}^{ab} in such defined model will be then:

$$C_{ij}^{ab} \equiv f_{ij}^{ab} - f_i^a f_j^b, \quad (\text{A1})$$

being a $qL \times qL$ matrix. As previously discussed, in [15], they introduced a further quantity, ϕ_i^a , called *positional information*, aimed at highlighting highly conserved positions with respect to the background amino acids frequencies within the correlation matrix. Let us define the background frequency of the a -th amino acid as $\nu^a = \frac{1}{L} \sum_{i=1}^L f_i^a$. The measure of how much the site i is biased towards one particular amino acid with respect to the background is given by the Kullback - Leibler divergence, $D_{KL}(f_i || \nu) = \sum_{a=1}^q f_i^a \log(\frac{f_i^a}{\nu^a})$. In [15], they rescaled the correlation matrix C_{ij}^{ab} with the $D_{KL}(f_i || \nu)$ variation with respect to f_i^a , i.e., $\phi_i^a \equiv \frac{\partial D_{KL}(f_i || \nu)}{\partial f_i^a}$, in the following way:

$$\tilde{C}_{ij}^{ab} = (f_{ij}^{ab} - f_i^a f_j^b) \phi_i^a \phi_j^b. \quad (\text{A2})$$

In order to avoid singularities due to the presence of the logarithm in the Kullback-Leibler divergence, we used pseudo counts to regularize frequencies [5, 9], i.e., adding at each position a fictive count.

Yet, due to projects focused on particular sequencings and the recent big advances in this field [18–20], sampling is not spatiotemporally homogenous and hence datasets are enriched of some specific very similar sequences. Then, to prevent biases due to over sampling, sequences have been reweighed by collapsing those overlapping at least of the 80%, which we will refer to as *similarity threshold* σ . However, any value $0.8 \leq \sigma \leq 1$ does not drastically change the results for the families we analyzed. In the following we shall call the number of effective sequences M_{eff} .

Regularization and reweighing can be expressed in a compact manner for single and double frequencies as it follows:

$$f_i^a = \frac{1}{M_{eff} + \lambda M_{eff}} \left(\frac{\lambda}{q} + \sum_{\alpha=1}^{M_{eff}} \delta_{a,s_i^\alpha} \right) \quad (\text{A3})$$

and

$$f_{ij}^{ab} = \frac{1}{M_{eff} + \lambda M_{eff}} \left[\frac{\lambda}{q} \delta_{ij} \delta_{ab} + \frac{\lambda}{q^2} (1 - \delta_{ij}) + \sum_{\alpha=1}^N \delta_{a,s_i^\alpha} \delta_{b,s_j^\alpha} \right], \quad (\text{A4})$$

where $\lambda = 1$ is the pseudo count.

The regularized and reweighed \tilde{C}_{ij}^{ab} is still a $qL \times qL$ matrix: to reduce it to a $L \times L$ matrix, we used the so-called *Frobenius norm*, i.e.:

$$\bar{C}_{ij} = \sqrt{\sum_{a,b=1}^q \tilde{C}_{ij}^{ab}{}^2} \quad (\text{A5})$$

and normalized it with respect to the diagonal entries:

$$\hat{C}_{ij} \equiv \frac{\bar{C}_{ij}}{\sqrt{\bar{C}_{ii} \bar{C}_{jj}}}. \quad (\text{A6})$$

\hat{C}_{ij} is now a $L \times L$ symmetric matrix. To perform SCA, as we previously discussed, one must compare the spectral properties (i.e., eigenvalues and eigenvectors' components) of the \hat{C}_{ij} with those of the correlation matrix got from the reshuffled dataset. Data reshuffling is performed constraining on the single amino acid frequency at each site, i.e., randomly exchanging two different amino acids at the same position i . The procedure to compute the correlation matrix is exactly the same as before and we call the random matrix \mathcal{M}_{ij} .

As introduced in Sec.III D, to figure out whether some relevant information is enclosed in the dataset, one has firstly to compare eigenvalues' distributions relatively to the \hat{C}_{ij} with those of \mathcal{M}_{ij} . We expect \mathcal{M}_{ij} 's eigenvalues distribution to be Marchenko-Pastur like [36], i.e., a bulk of very small eigenvalues and short tails. Fig. 5a shows at least four eigenvalues (black blocks) of the \hat{C}_{ij} computed for the PF00072 rising out of the random bulk (orange blocks). The first highest eigenvalue has not been shown since it is a consequence of the phylogenetic history characterizing the dataset [15] and of the use of pseudo counts and it will not be taken into account for sectors selection. In order to identify *sectors*, we stucked with the second and third highest eigenvalues, λ_2 and λ_3 (Fig. 5a) and their associated eigenvectors, $|2\rangle$ and $|3\rangle$. The aim is to display those sites giving *signals* along these directions, i.e., having a projection along the two eigenvectors significantly higher than the random one. To define a discrimination threshold ϵ , we used the inverse participation ratios (Fig. 14) associated to each mode as well as the distribution of the eigenvectors' components (Fig. 12) for both the \hat{C}_{ij} and the \mathcal{M}_{ij} . The inverse participation ratio associated to the n -th mode, IPR_n , is defined as:

$$IPR_n = \sum_{i=1}^L (\langle i|n \rangle)^4 \quad (\text{A7})$$

and it gives a measure of the localization or delocalization of the eigenvectors' components. In Fig. 14 we show IPR_n for all the modes related to the actual and the random correlation matrix.

The imposed discrimination threshold is finally $\epsilon = 0.1$ for the PF00072. This allows to define sectors by clustering the selected sites in the plane spanned by $|2\rangle$ and $|3\rangle$ (Fig. 5b).

For PF00072, four sectors have been identified by grouping the positions in the plane spanned by $|3\rangle$ and $|2\rangle$, for instance in the following way:

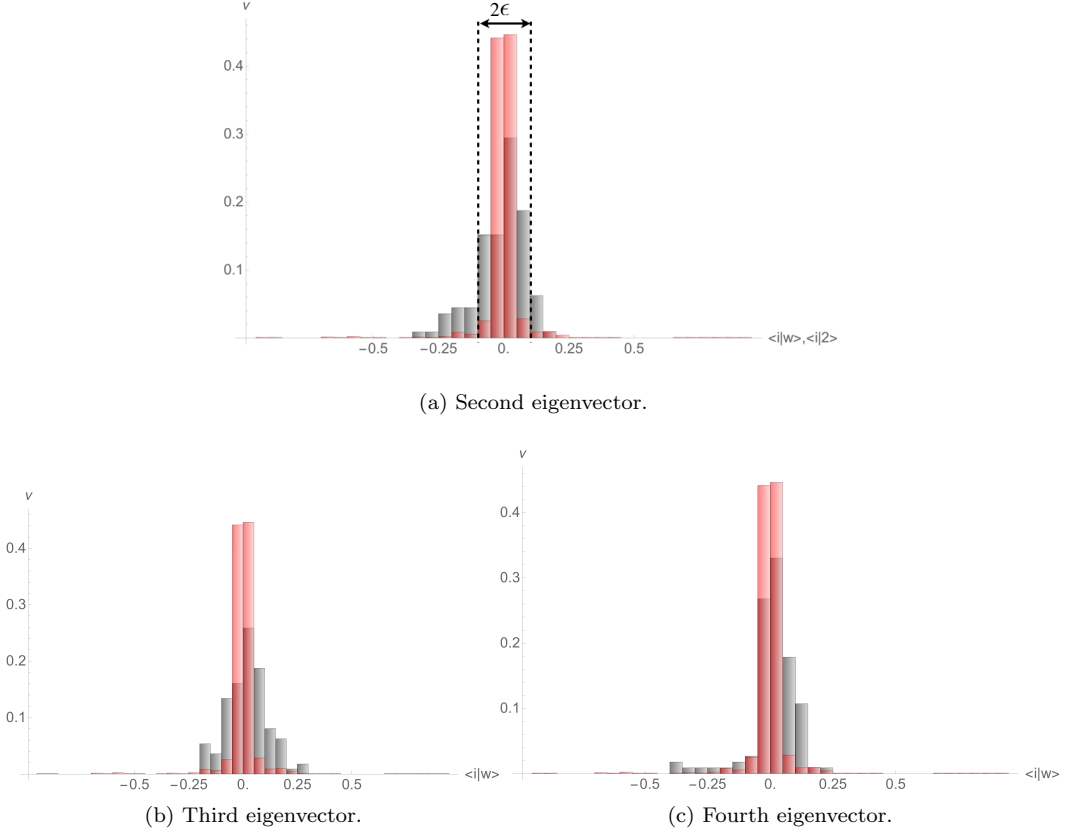


FIG. 12: Histograms of eigenvectors components frequencies, ν , relative to the correlation matrix \hat{C}_{ij} (black blocks) and to the random one (red blocks). In 12a the chosen threshold is plotted upon the histogram as well.

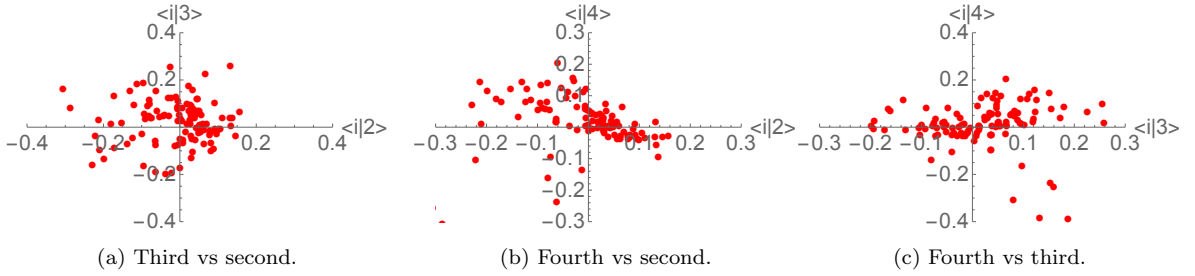


FIG. 13: Eigenvectors components for the matrix \hat{C}_{ij} . While in Fig. 13a one can still see a clusters structure, in the others the eigenvectors' components are much noisier.

- the first sector is identified by all those positions $\langle i|2\rangle > \epsilon$ and $|\langle i|2\rangle| > |\langle i|3\rangle|$;
- the second sector is identified by all those positions $\langle i|2\rangle < -\epsilon$ and $|\langle i|2\rangle| > |\langle i|3\rangle|$;
- the third sector is identified by all those positions $\langle i|3\rangle > \epsilon$ and $|\langle i|2\rangle| < |\langle i|3\rangle|$;
- the fourth sector is identified by all those positions $\langle i|3\rangle < -\epsilon$ and $|\langle i|2\rangle| < |\langle i|3\rangle|$.

The obtained sectors are shown in Fig. 6a and their meaning is widely discussed in the Main Text. In our analysis, however, we did not really use this discrimination threshold but we have rather ranked the SCA sites according to

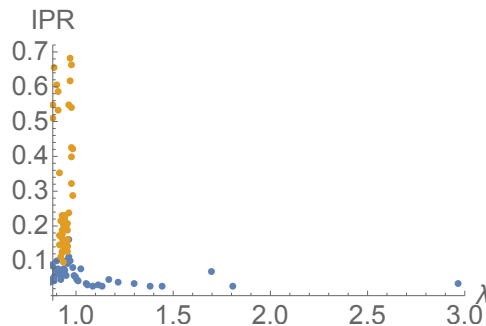


FIG. 14: Inverse participation ratios as a function of the eigenvalues for both the random matrix (orange) and the non-random one (blue).

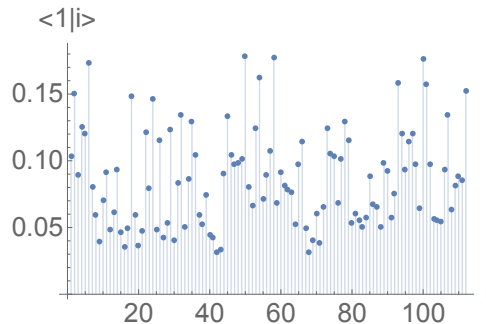


FIG. 15: First eigenvector components, $\langle 1|i\rangle$, plotted along the sequence. Notice that most of them are at least higher than 0.05.

their distance from the origin in the plane spanned by $|2\rangle$ and $|3\rangle$. The list of relevant sites has been built up by maximizing the overlap with the CVS results.

In our analysis we just stuck with the two highest eigenvalues of the correlation matrix. Yet, as pointed out in [10], smaller eigenvalues can still give signals about some positions. However, we found that CVS recovers most of these positions found to be relevant along eigenvectors associated to smaller eigenvalues.

Appendix B: Direct Coupling Analysis in a nutshell

Direct contact prediction from MSAs has recently been subject of intense research. Here we focus on the well-known method of Direct Coupling Analysis. As discussed in the Introduction, many approaches have been proposed so far some aimed at minimizing the detection of false positives while some others at weighing the gaps introduced by the alignments. Hereafter, we will refer to [9] where they introduced and tested the so-called naive Mean Field approach (nMFDCA) to infer the interactions between the amino acids (see Supplementary Materials for further details).

The ansatz of DCA methods is that each sequence is the outcome of a Boltzmann - distribution, $P(\vec{s})$, obtained from a maximum entropy principle under the constraints that marginal distributions must match the experimental ones, i.e.:

$$\begin{aligned} P(s_i = a) &\equiv f_i^a \\ &\text{and} \\ P(s_i = a, s_j = b) &\equiv f_{ij}^{ab}. \end{aligned}$$

This allows the introduction of a q-state Potts' hamiltonian, \mathcal{H} , given by:

$$\mathcal{H}[\vec{s}] = - \sum_{i < j} J_{ij}(s_i, s_j) - \sum_i h_i(s_i). \quad (\text{B1})$$

The model we are aimed at fitting data with is then a 21-state Potts' model.

Since for each site i frequencies sum up to 1, being there L constraints for each site, the model has $(q-1)L$ free parameters which can be inferred exploiting the Plefka's expansion of the Gibbs' free energy generalized to the q -state Potts' model: it relates couplings $J_{ij}(s_i, s_j)$ to the $(q-1)L \times (q-1)L$ correlation matrix $C_{ij}(s_i, s_j)$ [9, 33]. The correlation matrix $C_{ij}(s_i, s_j)$ is defined as in SCA other than the rescaling with positional conservation [37]. One can check that from the Plefka's expansion it follows that:

$$J_{ij}(s_i, s_j) = -(C_{ij}(s_i, s_j))^{-1}. \quad (\text{B2})$$

However, to ensure matrix inversion, one must neglect the q -th degree-of-freedom because of the L frequency constraints we discussed before. Here, the use of pseudo counts is fundamental in order to avoid singularities due to positional under sampling.

This allows to obtain a regular $J_{ij}(s_i, s_j)$ matrix whose dimensions are $(q-1)L \times (q-1)L$: to perform a dimensional reduction on the couplings and turning again to a $L \times L$ matrix, one can introduce again the q -th degree-of-freedom (as a null column/row) and then to standardize the couplings in the following way:

$$\tilde{J}_{ij}(s_i, s_j) = J_{ij}(s_i, s_j) - \mu_{ij}(s_i) - \mu_{ij}(s_j) + \mu_{ij}, \quad (\text{B3})$$

where $\mu_{ij}(s_i) = \frac{1}{L} \sum_{s_j=1}^q J(s_i, s_j)_{ij}$ (analogously for $\mu_{ij}(s_j)$) and $\mu_{ij} = \frac{1}{L^2} \sum_{s_i, s_j=1}^q J_{ij}(s_i, s_j)$ and then take the Frobenius norm as previously defined. The Frobenius norm computed on this new couplings matrix is called the *F-score*, defined as:

$$F_{ij} \equiv \|\tilde{J}_{ij}(s_i, s_j)\|_{s_i, s_j} = \sqrt{\sum_{s_i, s_j=1}^q J_{ij}(s_i, s_j)^2}. \quad (\text{B4})$$

The F-score turns out to have zero elements on the diagonal, i.e., zero self-couplings, and a better highlight of structures within the coupling matrix [10].